Biosensors and Bioelectronics 142 (2019) 111516

Contents lists available at ScienceDirect

Biosensors and Bioelectronics

journal homepage: www.elsevier.com/locate/bios

Photoelectrochemical biosensor for 5hmC detection based on the photocurrent inhibition effect of ZnO on MoS_2/C_3N_4 heterojunction

Chengji Sui[a], Fei Li[a], Hanwen Wu[c], Huanshun Yin[a,*], Shenran Zhang[a], Geoffrey I.N. Waterhouse[a,d], Jun Wang[b,**], Lusheng Zhu[b,***], Shiyun Ai[a]

[a] College of Chemistry and Material Science, Shandong Agricultural University, 271018, Taian, Shandong, PR China
[b] College of Resources and Environment, Key Laboratory of Agricultural Environment in Universities of Shandong, Shandong Agricultural University, Taian, 271018, PR China
[c] College of Chemistry and Chemical Engineering, Central South University, 410083, Changsha, Hunan, PR China
[d] School of Chemical Sciences, The University of Auckland, Auckland, 1142, New Zealand

ARTICLE INFO

Keywords:
DNA hydroxymethylation
Covalent chemical reaction
MoS_2/C_3N_4 heterojunction
Rice seedling
Photoelectrochemical biosensor

ABSTRACT

A novel photoelectrochemical biosensor was fabricated for 5-hydroxymethylcytosine (5hmC) detection based on the photocurrent inhibition effect of ZnO on MoS_2/C_3N_4 heterojunction. Firstly, the ITO electrode was modified successively with MoS_2 and g-C_3N_4 as photoelectric materials to deliver a strong photocurrent response. Next, the 5-hydroxymethyl group (-CH_2OH) of 5hmC was oxidized by $KRuO_4$ to produce an aldehyde group (-CHO), where 5hmC was converted into 5-formylcytosine (5fC). Based on the covalent reaction with between –CHO of 5fC and –NH_2 groups of g-C_3N_4, 5fC can be captured on electrode surface. Finally, the ZnO-PAMAM composite was covalently attached to the phosphate group of the immobilized 5fC, which could decrease the electron transfer amount of g-C_3N_4 to MoS_2, absorption of light and consumption of electron donors thereby resulting the decrease of photocurrent. Under optimal conditions, the photocurrent shows a linear relationship with the logarithm value of 5hmC concentration from 0.01-200 nM with a low detection limit of 2.6 pM. Moreover, this method was selective and allowed to discriminate between 5hmC and 5-methylcytosine (5mC) in DNA. Finally, the photoelectrochemical biosensor was successfully applied to investigate the effect of heavy metal ion and phytohormones on 5hmC expression in rice seedlings leaves.

1. Introduction

Cytosine demethylation plays an important role in the genomes of most plants and animals. In the demethylation reaction, 5-methylcytosine (5mC) is oxidized by 10–11 translocation proteins (Song et al., 2010), yielding 5-hydroxymethylcytosine (5hmC) as the main product, which is considered as the sixth base of DNA. Due to its prevalence at low concentrations in most plants and animal tissues, 5hmC is hypothesized to play crucial roles in gene regulation (Münzel et al., 2011). In order to understand the biological function of 5hmC, its detection in different tissues is needed. However, due to the low abundance and similar structure with 5mC, it is required that the detection method should be sensitive and selective.

Various methods have been developed for 5hmC detection, including fluorescence, single-molecule real-time sequencing, thin layer chromatography, high performance liquid chromatography-mass spectrometry, immunoassay, capillary electrophoresis, electrochemistry, electrochemiluminescence and photoelectrochemistry (Branco et al., 2011; Chen et al., 2017; Flusberg et al., 2010; Krais et al., 2011; Liu et al., 2019; Wang et al. 2019a, 2019c). Among these methods, photoelectrochemical technique has attracted more attentions due to the advantages of simplicity, inexpensive instrument, ease of miniaturization, low background signal and high sensitivity (Zhao et al., 2014). Based on these advantages, photoelectrochemical biosensors have received many attentions in recent years, which have been applied to detect different target, such as microRNA (Hou et al., 2018), acetylcholinesterase (Hou et al., 2016), ATP (Li et al., 2017a), oxytetracycline (Li et al., 2017c), thrombin (Hao et al., 2018), cell (Pang et al., 2016), glucose (Wu et al., 2017). We are excited that photoelectrochemical method also shows great potential for 5hmC detection (Sui

* Corresponding author.
** Corresponding author.
*** Corresponding author.
E-mail addresses: yinhs@sdau.edu.cn (H. Yin), jwang@sdau.edu.cn (J. Wang), lushzhu@sdau.edu.cn (L. Zhu).

https://doi.org/10.1016/j.bios.2019.111516
Received 24 April 2019; Received in revised form 5 July 2019; Accepted 13 July 2019
Available online 16 July 2019
0956-5663/ © 2019 Elsevier B.V. All rights reserved.

et al., 2019). Photoactive material is crucial for photoelectrochemical biosensor fabrication. To date, many semiconducting nanomaterials have been applied in photoelectrochemical assay, including g-C_3N_4 (Wang et al., 2019b), MoS_2 (Zang et al., 2016), WS_2 (Tan et al., 2018), ZnO (Lan et al., 2017), Bi_2S_3 (Okoth et al., 2016) and TiO_2 (Li et al., 2018). Among them, MoS_2, a kind of two-dimensional (2D) transition metal chalcogenides (TMCs), presents increasing application in photoelectrochemistry due to its unique physical, chemical and electronic properties. Moreover, MoS_2 can be not only easily functionalized to achieve high biomolecule loadings, but also easily dispersible in aqueous solutions, which is a key requirement for most biosensing applications (Mo et al., 2017). However, the high electron-hole recombination efficiency limits the application of MoS_2 in photoelectrochemical assay. To solve it, modification of MoS_2 with other photoactive material to form heterojunction structure is one of effective means. As a kind of metal-free semiconductor, graphite-like carbon nitride (g-C_3N_4) also receives widely attentions in photoelectrochemical catalysis and analysis due to the advantages of excellent visible photoactivity, relatively low band gap, high chemical and thermal stability, biocompatibility simple preparation, environmental friendliness, and inexpensive raw material (Masih et al., 2017). The combination of MoS_2 and g-C_3N_4 has been frequently used in photocatalysis as visible light catalyst because of their ideally matched energy levels, which can greatly improve the separation of photo-generated electron and hole of MoS_2 (Liu et al., 2018; Yuan et al., 2019).

Recently, many reports are focusing on signal-off photoelectrochemical biosensors with high detection sensitivity (Zhao et al., 2018). Most of the photoelectrochemical biosensors rely on steric-hinerance effect, which result from specific recognition between an antibody and antigen to block charge generation and electron transfer (Fan et al., 2016; Wang et al., 2015). For signal amplification in these photoelectrochemical biosensors, enzymatic reactions are commonly employed. However, the use of purified enzymes can greatly increase the cost of sensor fabrication, whilst also complicates the testing procedure, thereby narrowing the application of the biosensor. Thus, alternative signal amplification strategies are required. ZnO is a n-type semiconductor, which is now widely used in photoelectrochemical biosensors. However, ZnO is generally used as the photoactive material in most reports, rather than the signaling amplification unit. The conduction band and valence band positions of ZnO make it suitable as a signaling unit when attached to a photoelectrochemical biosensor platform based on a MoS_2/g-C_3N_4 heterojunction, motivating the development here of such a biosensor for the sensitive detection of 5hmC. In this work, we used the covalent reaction of 5hmC and the photocurrent inhibition effect of ZnO on a MoS_2/C_3N_4 heterojunction to achieve the sensitive and selective detection of 5hmC. To prove the applicability of this biosensor, the effects of heavy metals and phytohormones on the expression of 5hmC in rice seedling leaves were studied by the proposed method, which could provide new biomarker and new method for the evaluation of ecotoxicological effects of the above pollutants.

2. Experimental section

2.1. Reagents and apparatus

See Supplementary Material.

2.2. Preparation of MoS_2

MoS_2 nanosheets were prepared using a typical ultrasound method (Li et al., 2015). Firstly, 1 g of MoS_2 powder and 0.3 g of sodium cholate were added into 200 mL of distilled water. Then, the solution was sonicated for 20 h at room temperature. Afterwards, the dispersion was centrifuged at 3000 rpm for 15 min to remove any large MoS_2 pieces. Finally, the product was collected by centrifugation (12000 rpm) and washed three times with double distilled water and ethanol, respectively.

2.3. Preparation of g-C_3N_4

g-C_3N_4 was synthesized according to previous work (Li et al., 2017b). The preparation process was described in Supplementary Material.

2.4. Preparation of ZnO-PAMAM

See Supplementary materials.

2.5. Pretreatment of 5hm-dCTP

5hm-dCTP was oxidized by $KRuO_4$ to produce the 5fC according to previous work (Ma et al., 2016). Briefly, 10 μL of 1 mM $KRuO_4$ water solution was added into 200 μL of 10 μM 5hm-dCTP solution in an ice water bath, and the resulting solution kept at 0 °C for 1 h to afford 5fC. Excess $KRuO_4$ was removed using a dialysis membrane.

2.6. Biosensor fabrication

The ITO working electrode was cleaned via ultrasonic treatment in an ethanol/NaOH solution (v/v, 1:1), then acetone and finally double distilled water, and then air-dried. The electrode geometric area is about 0.196 cm^2. Aqueous dispersion of MoS_2 (4 mg/mL) and g-C_3N_4 (3 mg/mL) were prepared and subjected to ultrasound treatment for 30 min to achieve homogeneous dispersions. Then, 40 μL of the MoS_2 dispersion was dropped onto the bare ITO electrode surface and dried under the infrared lamp. The obtained electrode was denoted as MoS_2/ITO. Next, 40 μL of the g-C_3N_4 dispersion was dropped onto the MoS_2/ITO electrode surface and dried under the infrared lamp (The electrode was named as g-C_3N_4/MoS_2/ITO). Subsequently, 20 μL of the pretreated 5hm-dCTP solution was dropped onto the g-C_3N_4/MoS_2/ITO electrode surface and incubated at 37 °C in a humid environment for 2 h. The obtained modified electrode (denoted as 5fC/g-C_3N_4/MoS_2/ITO) was rinsed three times with washing buffer. Then, 40 μL of 100 nM formic acid solution was dropped onto the electrode, after which 40 μL of ZnO-PAMAM solution deposited on the 5fC/g-C_3N_4/MoS_2/ITO electrode and the resulting electrode kept at 37 °C in a humid environment for 105 min. The resulting electrode (ZnO/5fC/g-C_3N_4/MoS_2/ITO) was rinsed repeatedly with washing buffer and stored at 4 °C until photoelectrochemical tests.

2.7. Photoelectrochemical tests

Photoelectrochemical experiments were carried out on a home-built photoelectrochemical system, employed with a 500 W Xe lamp as the irradiation source. The wavelength range of the stimulation resource was 380–750 nm. However, to ensure the activity of biomolecules, we use filters to filter out the ultraviolet light during the experiment. So, the wavelength range of the stimulation resource was 420–750 nm in the experiment. Photoelectrochemical measurements were performed at a potential of −0.3 V in a detection buffer containing 0.1 M PBS and 0.1 M AA (pH = 7.4).

2.8. Real sample preparation

To test the applicability of the biosensor, the effects of Cd^{2+} ions, abscisic acid, 6-benzylaminopurine and 3-indoleacetic acid on 5hmC content in rice seedling leaves were investigated. The sample preparation process was as follows. Firstly, rice seeds were washed with distilled water and then soaked overnight in distilled water. Next, the seeds were germinated on a plastic tray. When the seedings had grown to a height of about 10 cm, the seedlings were soaked in distilled water

that contained different concentration of Cd^{2+}, abscisic acid, 6-benzylaminopurine or 3-indoleacetic acid. After seven days, the leaves were harvested and immediately frozen in liquid nitrogen to allow grinding to a fine powder. Subsequently, the genomic DNA in these leaves was extracted using a Plant Genomic DNA Extraction Kit (TianGen, Beijing, China) according to the manufacturer's instructions. The concentration of genomic DNA was measured using a Quawell Q5000 micro-volume UV spectrophotometer (USA). Finally, the genomic DNA was degraded to its individual nucleotide components by the catalytic effect of DNA Degradase™ (Zymo Research, USA).

3. Results and discussion

3.1. Detection strategy

In this work, a simple photoelectrochemical biosensor was proposed for the detection and quantification of single 5hmC base. The detection strategy is based on the specific oxidation of 5hmC to 5fC by $KRuO_4$, followed by reaction between the –CHO groups of 5fC and the $–NH_2$ groups of g-C_3N_4 (part of a photoelectrochemical g-C_3N_4/MoS_2/ITO electrode system). Reaction of ZnO-PAMAM with the phosphate group of 5fC introduced ZnO-PAMAM on electrode surface, which not only inhibited light reaching the g-C_3N_4/MoS_2 photoactive material, but also shared the denoted electron from electron donor of AA, thereby reducing the measured photoelectrochemical response. Scheme 1A shows the stepwise fabrication and operating principle of the photoelectrochemical biosensor for 5hmC. Firstly, MoS_2 is coated on an ITO electrode surface, followed by coating with g-C_3N_4. The g-C_3N_4 layer improved the photocurrent response of the MoS_2/ITO electrode and also serves as a linker to capture 5fC formed by the action of $KRuO_4$ oxidation of 5hmC. After 5fC is captured on the electrode, ZnO-PAMAM is further modified on the modified electrode through reaction between ZnO and the phosphate group of immobilized 5fC. Since the surface of zinc oxide has a large amount of hydroxyl groups, which can react with phosphate group. So, the ZnO can be captured on the surface of the electrode by the covalent bond reaction (Armelao et al., 2008; Han et al., 2017; Meinderink et al., 2019). Absorption of light and consumption of electron donors by ZnO-PAMAM (a photoactive material), coupled with steric hindrance effects from ZnO-PAMAM, significantly reduces the photocurrent of the 5fC/g-C_3N_4/MoS_2/ITO electrode. By this approach, the attenuation in the photoelectrochemical signal can be quantitatively correlated with the 5hmC concentration.

3.2. Characterization of materials

The materials used for photoelectrochemical biosensor fabrication were first characterized to examine their morphology and crystallinity. SEM, TEM and AFM reveals that the MoS_2 has a sheet structure (Fig. 1A, Fig. 1B and D), with the thickness of sheets being around 2 nm (i.e. around 3 MoS_2 nanosheet layers) (Tsai et al., 2014). All the diffraction peaks in the XRD pattern of the MoS_2 sample (Fig. 1E) can be indexed to hexagonal-phase MoS_2 (JCPDS card no. 65–7025) (Jiang et al., 2017). The g-C_3N_4 also possesses a sheet structure (Fig. 1C). Fig. 1F shows the characteristic (100) and (002) reflections of g-C_3N_4, which arise from in-plane structural packing of triazine units and stacking of the conjugated aromatic system, respectively. The XRD pattern of the ZnO sample (Fig. 1G) reveals the wurtzite hexagonal crystalline phase (JCPDS No. 36–3411) (Pirhashemi and Habibi-Yangjeh, 2017).

3.3. EIS and photoelectrochemical characterization of the biosensor

EIS is an excellent method for characterizing electrode modification process, which can effectively reflect the interface electron transfer resistance change with different modifications (thereby verifying whether a particular modification was successful or not). Here, EIS was employed to monitor each step of ZnO/5fC/g-C_3N_4/MoS_2/ITO biosensor construction. As shown in Fig. 2A, the electron transfer resistance (R_{et}) of the bare ITO electrode is about 260 Ω (curve a). When MoS_2 was coated on the ITO electrode, the R_{et} increases (curve b) which is attributed to negative charge on the surface of the MoS_2 nanosheets

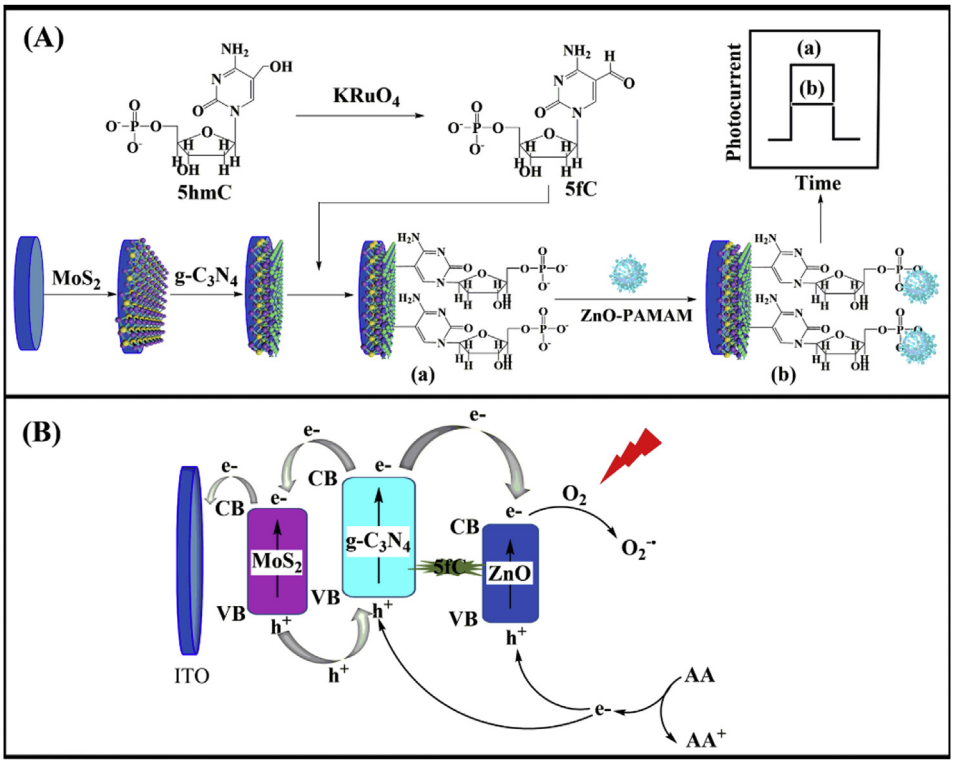

Scheme 1. (A) Construction process of the proposed photoelectrochemical biosensor, (B) Photogenerated electron-hole transfer mechanism of the photoelectrochemical biosensor for the detection of 5hmC.

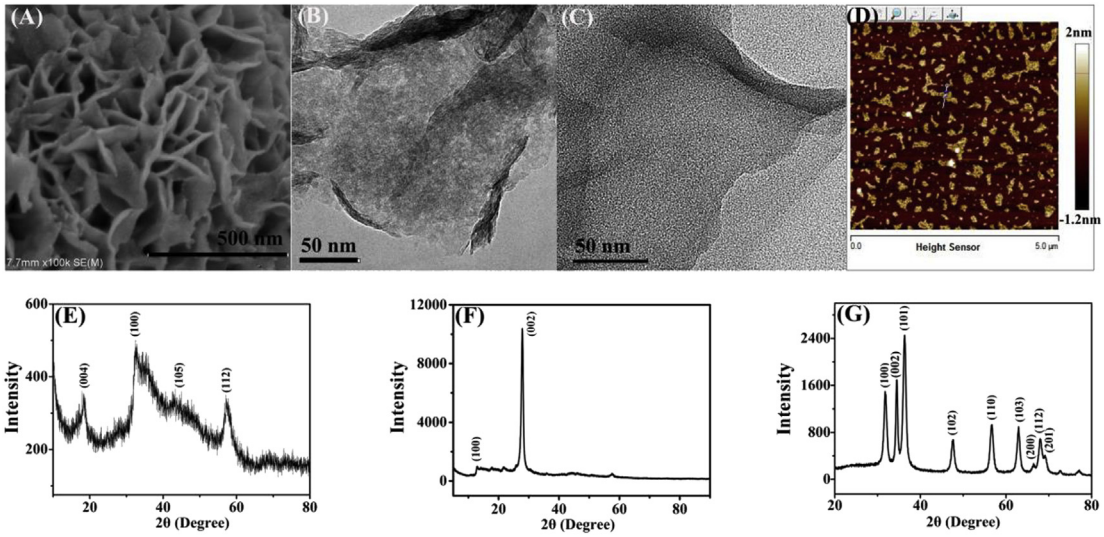

Fig. 1. (A) SEM image of MoS_2. TEM image of MoS_2 (B) and g-C_3N_4 (C). (D) AFM image of MoS_2. XRD pattern of MoS_2 (E), g-C_3N_4 and ZnO (F).

(repelling the $Fe(CN)_6^{3-/4-}$ redox probe) and the poor conductivity of MoS_2 nanosheets (Su et al., 2017). After g-C_3N_4 is captured on the electrode surface, the R_{et} value decreases (curve c) due to the amino groups (-NH_2) on g-C_3N_4 (Li et al., 2016), which may enhance the diffusion of the negatively charged redox probe of $Fe(CN)_6^{3-/4-}$ to electrode surface. Afterwards, the R_{et} value increased considerably (curve d) when 5f-dCTP is captured on the g-C_3N_4/MoS_2/ITO electrode surface. It is explained as the fact that the immobilized 5f-dCTP possesses phosphate group with negative charge, which hinders the diffusion of the redox probe of $Fe(CN)_6^{3-/4-}$ and causes an increased resistance. The introduction of ZnO-PAMAM further increases the R_{et} value (curve e) due to the bulky ZnO-PAMAM blocking electron transfer of the redox probe to 5fC/g-C_3N_4/MoS_2/ITO electrode, thereby increasing the charge transfer resistance. Moreover, the adsorption of ZnO-PAMAM was explained in detail in the supporting information. The EIS data in Fig. 2A thus confirms that each step in the biosensor fabrication process is successful.

In order to investigate the detection feasibility of the photoelectrochemical biosensor, the photocurrent response of the various modified electrodes were measured and compared. As shown in Fig. 2B, the photocurrent of the MoS_2/ITO electrode is about 520 nA (curve a), indicating that MoS_2 nanosheets possesses photoactivity. After coating g-C_3N_4, the photocurrent increases greatly (curve b). It clearly demonstrates that g-C_3N_4 can improve the photocurrent response of MoS_2 by facilitating charge separation and preventing electron-hole recombination, as depicted in Scheme 1B. However, the photocurrent decreases when the 5f-dCTP is captured on the surface of the g-C_3N_4/MoS_2/ITO electrode (curve c). This is explained by the steric hindrance effect and electrostatic repulsion effect of 5hm-dCTP, which decreases the transfer of the electron donor of AA to the surface of MoS_2/C_3N_4 heterojunction for reacting with the photo-generated holes. As a result, the recombination of electrons and holes is increased, which decreases the photocurrent. Subsequently, the photocurrent decreases strongly when ZnO-PAMAM is immobilized on the electrode surface (curve d). This can be rationalized in terms of steric hindrance of ZnO-PAMAM, as well as competitive absorption of light and consumption of electron donors by ZnO (Fan et al., 2016). To test the importance of 5hm-dCTP in ZnO-PAMAM capture, a control experiment was performed. Firstly, the g-C_3N_4/MoS_2/ITO electrode was incubated with ZnO-PAMAM, then washed three times with washing buffer. Photoelectrochemical performance of the resulting electrode (Fig. 2B, curve e) is similar to that of the g-C_3N_4/MoS_2/ITO electrode (Fig. 2B, curve b), offering a photocurrent much higher than that measured for the ZnO/5fC/g-C_3N_4/MoS_2/ITO electrode. This suggests that ZnO-PAMAM did not assemble on the electrode surface in the absence of 5f-dCTP. These results conclusively demonstrate that the biosensor could be used to detect 5hm-dCTP.

3.4. Optimization of detection conditions

See Supplementary Material.

The optimal results are as follows: MoS_2 concentration, 4.0 mg/mL; g-C_3N_4 concentration, 3.0 mg/mL; DNA immobilization time, 120 min; ZnO-PAMAM immobilization time, 105 min.

3.5. Performance of the biosensor for 5hm-dCTP detection

In order to verify the detection sensitivity of the biosensor, the

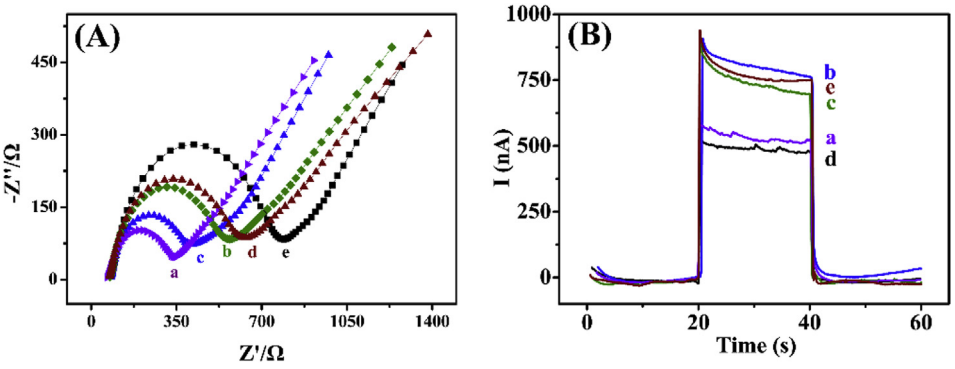

Fig. 2. (A) EIS of ITO (a), MoS_2/ITO (b), g-C_3N_4/MoS_2/ITO (c), 5fC/g-C_3N_4/MoS_2/ITO (d), ZnO/5fC/g-C_3N_4/MoS_2/ITO (e) in 5 mM K_3 [$Fe(CN)_6$]/K_4 [$Fe(CN)_6$] (1:1) containing 0.1 M KCl. (B) Photoelectrochemical response of MoS_2/ITO (a), g-C_3N_4/MoS_2/ITO (b), 5fC/g-C_3N_4/MoS_2/ITO (c), ZnO/5fC/g-C_3N_4/MoS_2/ITO (d), g-C_3N_4/MoS_2/ITO incubated with ZnO-PAMAM (e).

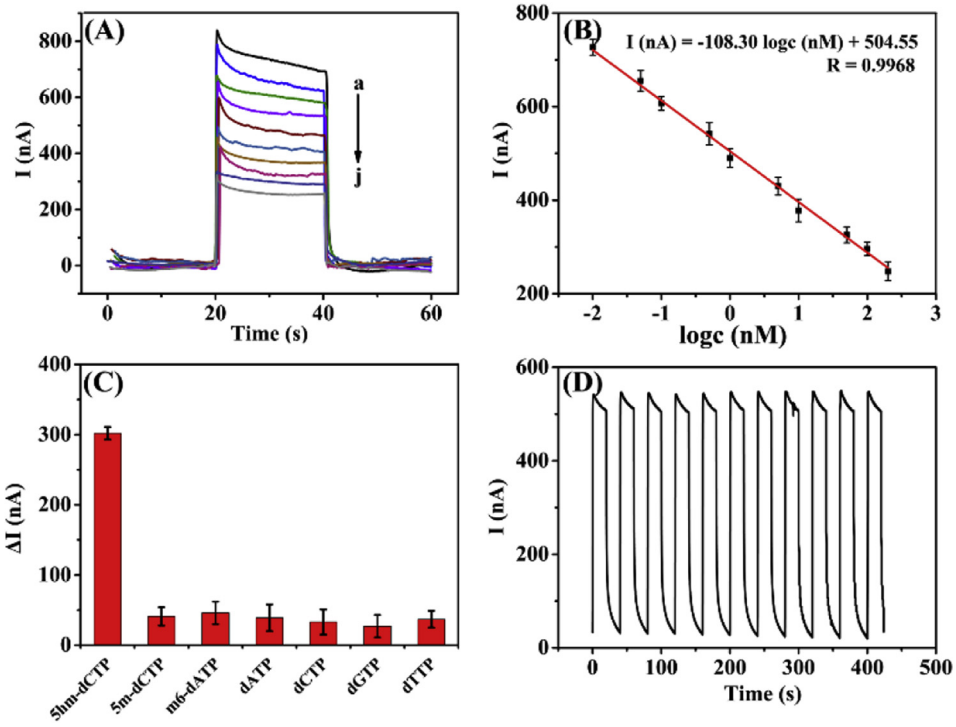

Fig. 3. (A) The photocurrent of the biosensor with different concentrations of 5hm-dCTP. (a–j) 0.01, 0.05, 0.1, 0.5, 1, 5, 10, 50, 100, 200 nM. (B) Plot of photocurrent versus the logarithm of the 5hm-dCTP concentration. (C) The photocurrent of the biosensor after it was incubated with different deoxyribonucleotides. (D) Time-based photocurrent responses of the biosensor during light on and light off cycles. Error bar was obtained by three measurements.

Table 1
Performance comparison of the photoelectrochemical biosensor with other methods developed for hydroxymethylated DNA detection.

Methods	Target	Linear range	Detection limit (pM)	Refs
Capillary electrophoresis	5hmC-DNA	0.09–90 nM	90	Krais et al. (2011)
Fluorescence	5hmC-DNA	0–100 nM	167	Chen et al. (2017)
Fluorescence	5hmC-DNA	–	0.035	Wang et al. (2018)
Electrochemiluminescence	5hmC-DNA	0.5–100 pM	0.14	Ma et al. (2016)
Electrochemiluminescence	5hmC-DNA	0.01–1000 pM	0.0038	Wei et al. (2017)
Electrochemiluminescence	5hmC-DNA	0.05–10 nM	16.3	Zhang et al. (2017)
Electrochemiluminescence	5hmC-DNA	0.05–10 pM	0.012	Sun et al. (2019)
Electrochemiluminescence	5hm-dCTP	0.1–30 nM	47	Jiang et al. (2018)
Electrochemistry	5hm-dCTP	0.1–30 nM	32	Yang et al. (2015)
Electrochemistry	5hmC-DNA	0.5–90 nM	140	Yin et al. (2017)
Electrochemistry	5hmC-DNA	0.01–1000 pM	0.009	Cui et al. (2019)
Photoelectrochemistry	5hm-dCTP	0.01–100 nM	4.12	Zhou et al. (2019)
Photoelectrochemistry	5hmC-DNA	0.5–100 nM	160	Yang et al. (2016)
Photoelectrochemistry	5hm-dCTP	0.01–200 nM	2.6	This work

photoelectrochemical response of the ZnO/5fC/g-C_3N_4/MoS_2/ITO biosensor was examined at different concentrations of 5hm-dCTP under the optimized testing conditions. As shown in Fig. 3A, the photocurrent decreases with increasing 5hm-dCTP concentration from 0.01 to 200 nM. The photocurrent response is proportional to the logarithm value of 5hm-dCTP concentration (Fig. 3A). The linear regression equation is I (nA) = −108.30 log$c$ (nM) + 504.55 (R = 0.9968) with the detection limit of 0.0026 nM (S/N = 3) (Fig. 3B). Table 1 compares the detection performance of the ZnO/5fC/g-C_3N_4/MoS_2/ITO biosensor with other reported sensors for 5hmC detection. The comparison reveals the photoelectrochemical biosensor developed in this work offers a wider linear range and lower detection limit than other sensors reported to date for 5hmC. Though some detection limits obtained by other work are lower than our work, however, the detection target for these work is DNA sequence containing 5hmC, which cannot achieve the single 5hmC base detection.

The selectivity, stability and reproducibility of the biosensor towards 5hm-dCTP was also investigated. To investigate the selectivity of the biosensor, dATP, dTTP, dGTP, dCTP, 5m-dCTP, m6-dATP were used as the possible potential interferants. In these experiments, 1 nM 5hm-dCTP was replaced by the same concentration of the potential interferant and the photocurrent change was compared ($\Delta I = I_2 - I_1$, where I_2 is the photocurrent of g-C_3N_4/MoS_2/ITO, and I_1 is the g-C_3N_4/MoS_2/ITO after incubation with different deoxyribonucleotides and ZnO-PAMAM, where the deoxyribonucleotides were also pretreated with $KRuO_4$). As shown in Fig. 3C, the photocurrent change of the biosensor incubated with 5hm-dCTP was much greater than that of biosensors fabricated using the other deoxyribonucleotides. Thus, it can be concluded that the biosensor possessed good detection selectivity. Since 5hmC was converted to 5fC to achieve the sensitive detection of 5hmC, which can absolutely cause the interference from the original 5fC in genomic DNA. To eliminate this interference, the following strategy can be employed. Firstly, the original 5fC concentration (C_1) is detected using our PEC detection strategy, in which the step for $KRuO_4$ oxidation is not performed. Then, the total 5fC concentration (C_2) is detected after $KRuO_4$ oxidation treatment using our PEC detection strategy. 5hmC concentration is then be calculated with the equation of C=C_2–C_1. Based on the above analysis, we think that our detection strategy can well discriminate 5hmC and other nucleotides, and presents good detection specificity.

Biosensor stability is another important performance metric. This was examined by studying the photocurrent response of the ZnO/5fC/g-C_3N_4/MoS_2/ITO electrode over 11 successive light on and light off cycles over 440 s. As shown in Fig. 3D, no significant change in the photocurrent response is observed, with the relative standard deviation (RSD) of the photoelectrochemical response being only 1.45%, indicating that the biosensor possesses excellent operational stability. The reproducibility of the biosensor was also investigated by comparing the photocurrent of seven ZnO/5fC/g-C_3N_4/MoS_2/ITO electrodes fabricated at the same time. No significant differences are found in the photocurrent of the seven independent photoelectrochemical biosensors (RSD 2.46%), indicating good reproducibility. Moreover, the performance of the g-C_3N_4/MoS_2/ITO electrode was also investigated in the supporting information.

3.6. Detection of 5hmC in samples

To further evaluate the potential of the biosensor for 5hmC detection, the effects of heavy metal ion (Cd^{2+}), three typical phytohormones (Abscisic acid, 6-benzylaminopurine and 3-indoleacetic acid, which belong to three typical kinds of phytohormones, that is Abscisic acid, Cytokinin and Auxins, respectively) on the 5hmC content in rice seedling leaves were investigated using this biosensor. The extensive use of heavy metal and phytohormone can cause serious environmental pollution, and then affect crop growth. In order to study the ecotoxicological effects of heavy metal and phytohormone, accurate method and appropriate evaluation indicator are needed. Therefore, 5hmC was employed as an alternative indicator and photoelectrochemical method was used as a new technique. As shown in Fig. 4A, the relative expression of 5hmC decreases with Cd^{2+} concentration up to 100 mg/L (the highest concentration studied). These results provide important information about the effect of heavy metal ions on the development of rice. Fig. 4B shows that the relative expression of 5hmC decreases with abscisic acid concentration in the examined concentration range of 0–5000 μM. The effects of 6-benzylaminopurine and 3-indoleacetic acid are similar to that of abscisic acid (Fig. 4C and D, respectively). The results in Fig. 4 are consistent with those determined using the MethylFlash Global DNA Hydroxymethylation (5hmC) ELISA Easy Kit (Epigentek, USA). These investigations prove that the fabricated biosensor possesses wide potential for 5hmC detection in real world samples.

4. Conclusion

In summary, a simple and sensitive photoelectrochemical biosensor was developed for 5hmC detection based on the covalent reaction and the photocurrent inhibition effect of ZnO on MoS_2/C_3N_4 heterojunction. The fabricated biosensor offers a wide linear detection range (0.01–200 nM), a low detection limit (2.6 pM), excellent selectivity (able to readily discriminate 5hmC and 5mC), excellent stability and good reproducibility. The photoelectrochemical biosensor allows 5hmC detection in the rice seedling leaves, which could provide new biomarkers and new methods for the evaluation of ecotoxicological effects of the heavy metal and phytohormones.

Declaration of competing interest

The authors declare that they have no known competing financial interests or personal relationships that could have appeared to influence the work reported in this paper.

Conflict of interest

We declare that we have no financial and personal relationships with other people or organizations that can inappropriately influence our work, there is no professional or other personal interest of any nature or kind in any product, service and/or company that could be construed as influencing the position presented in, or the review of, the manuscript entitled.

CRediT authorship contribution statement

Chengji Sui: Conceptualization, Data curation, Formal analysis, Investigation, Methodology, Writing - original draft. **Fei Li:**

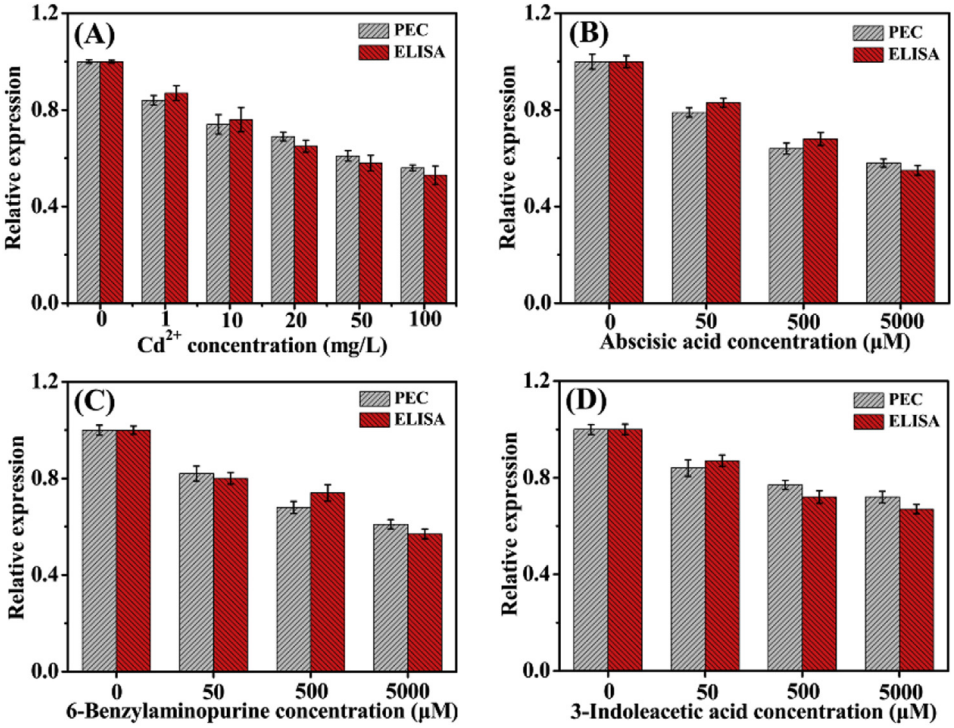

Fig. 4. Effect of Cd^{2+} (A), abscisic acid (B), 6-benzylaminopurine (C) and 3-indoleacetic acid (D) on 5hmC expression in the genomic DNA of rice seedling leaves.

Conceptualization, Data curation, Formal analysis, Investigation, Methodology, Writing - original draft. **Hanwen Wu:** Data curation, Formal analysis, Investigation, Methodology, Validation. **Huanshun Yin:** Conceptualization, Data curation, Investigation, Methodology, Project administration, Funding acquisition, Supervision, Writing - review & editing. **Shenran Zhang:** Conceptualization, Data curation, Formal analysis, Validation. **Geoffrey I.N. Waterhouse:** Formal analysis, Writing - review & editing. **Jun Wang:** Resources, Supervision, Funding acquisition, Writing - review & editing. **Lusheng Zhu:** Resources, Supervision, Funding acquisition, Writing - review & editing. **Shiyun Ai:** Resources, Supervision, Funding acquisition.

Acknowledgments

This work was supported by the National key research and development project of China (2018YFC1800605), the National Natural Science Foundation of China (Nos. 21775090, 41807484), the Natural Science Foundation of Shandong Province of China (Nos. ZR2016BM10 and ZR2018MB028). GINW acknowledges funding support from the MacDiarmid Institute for Advanced Materials and Nanotechnology.

Appendix A. Supplementary data

Supplementary data to this article can be found online at https://doi.org/10.1016/j.bios.2019.111516.

References

Armelao, L., Pascolini, M., Biasiolo, E., Tondello, E., Bottaro, G., Carbonare, M.D., D'Arrigo, A., Leon, A., 2008. Inorg. Chim. Acta 361, 3603–3608.
Branco, M.R., Ficz, G., Reik, W., 2011. Nat. Rev. Genet. 13, 7.
Chen, H.-y., Wei, J.-R., Pan, J.-X., Zhang, W., Dang, F.-q., Zhang, Z.-Q., Zhang, J., 2017. Biosens. Bioelectron. 91, 328–333.
Cui, L., Hu, J., Wang, M., Li, C.-c., Zhang, C.-y., 2019. Anal. Chem. 91, 1232–1236.
Fan, G.-C., Zhu, H., Du, D., Zhang, J.-R., Zhu, J.-J., Lin, Y., 2016. Anal. Chem. 88, 3392–3399.
Flusberg, B.A., Webster, D.R., Lee, J.H., Travers, K.J., Olivares, E.C., Clark, T.A., Korlach, J., Turner, S.W., 2010. Nat. Methods 7, 461.
Han, Z., Luo, M., Chen, L., Pan, H., Chen, J., Li, C., 2017. Microchim. Acta. 184, 2541–2549.
Hao, N., Hua, R., Chen, S., Zhang, Y., Zhou, Z., Qian, J., Liu, Q., Wang, K., 2018. Biosens. Bioelectron. 101, 14–20.
Hou, T., Xu, N., Wang, W., Ge, L., Li, F., 2018. Anal. Chem. 90, 9591–9597.
Hou, T., Zhang, L., Sun, X., Li, F., 2016. Biosens. Bioelectron. 75, 359–364.
Jiang, D., Du, X., Zhou, L., Li, H., Wang, K., 2017. Anal. Chem. 89, 4525–4531.
Jiang, W., Wu, L., Duan, J., Yin, H., Ai, S., 2018. Biosens. Bioelectron. 99, 660–666.
Krais, A.M., Park, Y.J., Plass, C., Schmeiser, H.H., 2011. Epigenetics 6, 560–565.
Lan, F., Liang, L., Zhang, Y., Li, L., Ren, N., Yan, M., Ge, S., Yu, J., 2017. ACS Appl. Mater. Interfaces 9, 37839–37847.
Li, B.L., Zou, H.L., Lu, L., Yang, Y., Lei, J.L., Luo, H.Q., Li, N.B., 2015. Adv. Funct. Mater. 25, 3541–3550.
Li, L., Wang, T., Zhang, Y., Xu, C., Zhang, L., Cheng, X., Liu, H., Chen, X., Yu, J., 2018. ACS Appl. Mater. Interfaces 10, 14594–14601.
Li, M.-J., Zheng, Y.-N., Liang, W.-B., Yuan, R., Chai, Y.-Q., 2017a. ACS Appl. Mater. Interfaces 9, 42111–42120.
Li, S., Dong, G., Hailili, R., Yang, L., Li, Y., Wang, F., Zeng, Y., Wang, C., 2016. Appl. Catal. B Environ. 190, 26–35.
Li, X., Zhu, L., Zhou, Y., Yin, H., Ai, S., 2017b. Anal. Chem. 89, 2369–2376.
Li, Y., Tian, J., Yuan, T., Wang, P., Lu, J., 2017c. Sens. Actuators B Chem. 240, 785–792.
Liu, Y., Siejka-Zielińska, P., Velikova, G., Bi, Y., Yuan, F., Tomkova, M., Bai, C., Chen, L., Schuster-Böckler, B., Song, C.-X., 2019. Nat. Biotechnol. 37, 424–429.
Liu, Y., Zhang, H., Ke, J., Zhang, J., Tian, W., Xu, X., Duan, X., Sun, H., Tade, M.O., Wang, S., 2018. Appl. Catal. B Environ. 228, 64–74.
Münzel, M., Globisch, D., Carell, T., 2011. Angew. Chem. Int. Ed. 50, 6460–6468.
Ma, S., Sun, H., Li, Y., Qi, H., Zheng, J., 2016. Anal. Chem. 88, 9934–9940.
Masih, D., Ma, Y., Rohani, S., 2017. Appl. Catal. B Environ. 206, 556–588.
Meinderink, D., Orive, A.G., Ewertowski, S., Giner, I., Grundmeier, G., 2019. ACS Appl. Nano Mater. 2, 831–843.
Mo, L., Li, J., Liu, Q., Qiu, L., Tan, W., 2017. Biosens. Bioelectron. 89, 201–211.
Okoth, O.K., Yan, K., Liu, Y., Zhang, J., 2016. Biosens. Bioelectron. 86, 636–642.
Pang, X., Zhang, Y., Pan, J., Zhao, Y., Chen, Y., Ren, X., Ma, H., Wei, Q., Du, B., 2016. Biosens. Bioelectron. 77, 330–338.
Pirhashemi, M., Habibi-Yangjeh, A., 2017. J. Colloid Interface Sci. 491, 216–229.
Song, C.-X., Szulwach, K.E., Fu, Y., Dai, Q., Yi, C., Li, X., Li, Y., Chen, C.-H., Zhang, W., Jian, X., Wang, J., Zhang, L., Looney, T.J., Zhang, B., Godley, L.A., Hicks, L.M., Lahn, B.T., Jin, P., He, C., 2010. Nat. Biotechnol. 29, 68.
Su, S., Cao, W., Liu, W., Lu, Z., Zhu, D., Chao, J., Weng, L., Wang, L., Fan, C., Wang, L., 2017. Biosens. Bioelectron. 94, 552–559.
Sui, C., Wang, T., Zhou, Y., Yin, H., Meng, X., Zhang, S., Waterhouse, G.I.N., Xu, Q., Zhuge, Y., Ai, S., 2019. Biosens. Bioelectron. 127, 38–44.
Sun, H., Wang, H., Bai, W., Bao, L., Lin, J., Li, Y., 2019. Talanta 191, 350–356.
Tan, Y., Li, M., Ye, X., Wang, Z., Wang, Y., Li, C., 2018. Sens. Actuators B Chem. 262, 982–990.
Tsai, M.-L., Su, S.-H., Chang, J.-K., Tsai, D.-S., Chen, C.-H., Wu, C.-I., Li, L.-J., Chen, L.-J., He, J.-H., 2014. ACS Nano 8, 8317–8322.
Wang, G.-L., Shu, J.-X., Dong, Y.-M., Wu, X.-M., Li, Z.-J., 2015. Biosens. Bioelectron. 66, 283–289.
Wang, H., Liu, M., Bai, W., Sun, H., Li, Y., Deng, H., 2019a. Sens. Actuators B Chem. 284, 236–242.
Wang, M., Yin, H., Zhou, Y., Sui, C., Wang, Y., Meng, X., Waterhouse, G.I.N., Ai, S., 2019b. Biosens. Bioelectron. 128, 137–143.
Wang, Y., Zhang, X., Wu, F., Chen, Z., Zhou, X., 2019c. Chem. Sci. 10, 447–452.
Wang, Z.-y., Wang, M., Zhang, Y., Zhang, C.-y., 2018. Chem. Commun. 54, 8602–8605.
Wei, Y., Sun, H., Li, J., Zhang, Y., Li, Y., Lin, J., Wang, T., Zhou, M., 2017. J. Electroanal. Chem. 795, 123–129.
Wu, S., Huang, H., Shang, M., Du, C., Wu, Y., Song, W., 2017. Biosens. Bioelectron. 92, 646–653.
Yang, Z., Jiang, W., Liu, F., Zhou, Y., Yin, H., Ai, S., 2015. Chem. Commun. 51, 14671–14673.
Yang, Z., Shi, Y., Liao, W., Yin, H., Ai, S., 2016. Sens. Actuators B Chem. 223, 621–625.
Yin, H., Yang, Z., Wang, H., Zhou, Y., Ai, S., 2017. Sens. Actuators B Chem. 243, 602–608.
Yuan, Y.-J., Shen, Z., Wu, S., Su, Y., Pei, L., Ji, Z., Ding, M., Bai, W., Chen, Y., Yu, Z.-T., Zou, Z., 2019. Appl. Catal. B Environ. 246, 120–128.
Zang, Y., Lei, J., Hao, Q., Ju, H., 2016. Biosens. Bioelectron. 77, 557–564.
Zhang, Y., Li, Y., Wei, Y., Sun, H., Wang, H., 2017. Talanta 170, 546–551.
Zhao, W.-W., Xu, J.-J., Chen, H.-Y., 2014. Chem. Rev. 114, 7421–7441.
Zhao, W.-W., Xu, J.-J., Chen, H.-Y., 2018. Anal. Chem. 90, 615–627.
Zhou, Y., Yin, H., Sui, C., Wang, Y., Ai, S., 2019. Chem. Eng. J. 357, 94–102.